NJC

ROYAL SOCIETY OF CHEMISTRY

PAPER

View Article Online
View Journal | View Issue

Cite this: *New J. Chem.*, 2025, **49**, 20847

Upgrading the ferribactin pre-chromophore – synthesis, modification and polymerization

Andreas P. Greulich,[a] M. Trisha C. Ang,[b] Diana Camila Munoz Castillo,[c] Brigitte Pawletta,[c] Stefan Hupke,[a] Büşra Nur Gür,[a] Isabell Muth,[a] Anna Zens,[a] Ursula Bilitewski,*[c] Matthias Bierenstiel *[b] and Sabine Laschat *[a]

Received 12th August 2025,
Accepted 15th November 2025

DOI: 10.1039/d5nj03251b

rsc.li/njc

The global rise in antibiotic resistance underscores the urgent need for alternative antimicrobial strategies. One approach involves the conjugation of iron-chelating moieties to macromolecular scaffolds to disrupt bacterial iron homeostasis and inhibit cellular uptake mechanisms. In this work, the pre-chromophoric unit of the siderophore ferribactin served as the structural template for the development of antimicrobial polymer precursors. A series of L-tyrosine and L-DOPA-derived pre-chromophore analogues were synthesized and chemically modified to introduce polymerizable functionalities. These monomers were copolymerized with *N*-vinylpyrrolidone *via* reversible addition–fragmentation chain-transfer (RAFT) polymerization to afford well-defined, bifunctional copolymers. Antimicrobial testing of the monomers and polymers showed varying levels of activity, depending on the bacterial species.

1. Introduction

The increase in antimicrobial resistance is a serious threat to human health causing an estimated 1.27 million annual deaths worldwide.[1–3] Therefore, the issue is under ongoing surveillance and discussion in the scientific and health communities.[1–3] Different approaches to combat these resistances are being pursued, including new technologies like artificial intelligence (AI),[3,4] or targeting enzymes in cell wall synthesis or in respiratory chain processes.[5,6] Other strategies focus on reducing the pathogenicity and virulence of bacteria rather than killing them to avoid selective evolutionary pressures, thus reducing the spread of antibiotic resistance by "diluting" the bacterial gene pool.[7–9] Targeting the nutrient supply of bacteria, such as the iron uptake, is another promising strategy to inhibit bacterial growth, especially in combination with antibiotics.[10]

Iron as a stoichiometric building block is an essential element in the bacterial growth phase. Nature developed various chelators for iron uptake, among which enterobactin **1** is a prominent example (Fig. 1). Enterobactin **1** belongs to a class of small iron chelating molecules named siderophores, produced by bacteria to maintain iron uptake, especially in iron deficient conditions.[10–12] Conjugates of siderophores and antibiotics show promising results as "Trojan horses", increasing the activity of antibiotics by using the bacteria's own pathways to bring antibiotics into the cell thus circumventing some bacterial resistance mechanisms.[13,14] Pyoverdin D **2** is an example for a class of siderophores used by the *Pseudomonas* species that has been thoroughly investigated.[15–21] The first total synthesis of pyoverdin D **2** was reported in 2013 by Mashiach and Meijler.[22] Synthetic approaches towards the chromophore unit **3-chr** of pyoverdin D **2** (marked blue in Fig. 1) have been known since 1990, but challenges remain due to the multistep syntheses and toxic reagents required.[23–25]

Ferribactin **4-ferri**, *i.e.* the biosynthetic precursor of pyoverdin **3-pyo**, is a weaker siderophore,[26] which is also found in *Pseudomonas* supernatants.[21] Ferribactin **4-ferri** differs from pyoverdin **3-pyo** only in the chromophore unit. Although some literature refers to the ferribactin substructure **4-chr** as a chromophore,[27–29] it should be noted that **4-chr** is a colorless compound. Therefore, in this work, unit **4-chr** is referred to as a pre-chromophore. Ferribactin **4-ferri** has been less studied than pyoverdin **3-pyo**, presumably due to the fact, that its binding affinity towards Fe(III) is 4 orders of magnitude lower than that of the corresponding Fe(III)-pyoverdin complexes. This vast difference is caused by the varying amounts of binding sites. Both siderophores have two binding sites in the form of *N*-formyl-*N*-hydroxy-L-ornithine moieties (marked pink in Fig. 1). But while the catechol unit of the pyoverdin chromophore **3-chr** provides a third binding site of pyoverdin, the phenol unit of

[a] *Institut für Organische Chemie, Universität Stuttgart, D-70569 Stuttgart, Germany. E-mail: sabine.laschat@oc.uni-stuttgart.de*
[b] *Department of Chemistry, Cape Breton University, 1250 Grand Lake Road, Sydney B1P 6L2, Nova Scotia, Canada. E-mail: trisha_ang@cbu.ca, matthias_bierenstiel@cbu.ca*
[c] *Helmholtz-Zentrum für Infektionsforschung (HZI) Braunschweig, Inhoffenstraße 7, D-38124 Braunschweig, Germany. E-mail: ursula.bilitewski@helmholtz-hzi.de*

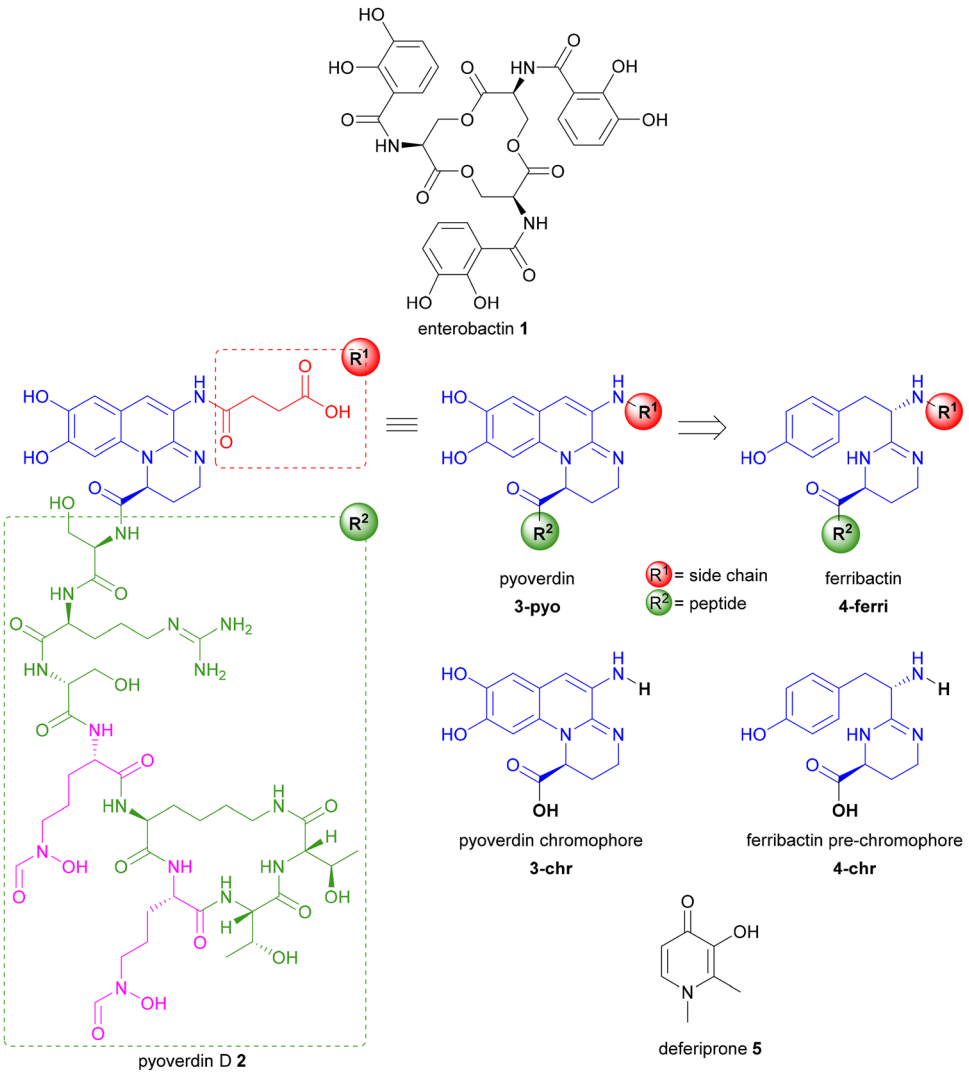

Fig. 1 Examples of siderophores, the (pre)chromophoric subunits of pyoverdin **3-chr** and ferribactin **4-chr** as well as deferiprone **5**.

the ferribactin pre-chromophore **4-chr** does not participate in complexation. This was shown by Budzikiewicz with ^{13}C NMR studies of Ga(III)-complex analogues of ferribactin compared with data for pyoverdin **3-pyo** from other literature.[26] Ga(III) serves as a substitute for Fe(III) with equal charge and comparable ion radius and does not have the unfavorable paramagnetic property afflicting NMR studies.[26] Most publications deal with the structure of ferribactin **4-ferri** and its role as precursor in the biosynthesis of pyoverdin **3-pyo**.[26–29] The synthesis of the ferribactin pre-chromophore **4-chr** was reported in 1993 by Jones, who achieved the formation of a tetrahydropyrimidine unit in **4-chr** *via* a chiral iminothioester.[30] However, epimerization occurred during the synthetic reaction and only a diastereomeric mixture was obtained.[30] Later, Abdallah performed the coupling *via* an amide and Meerwein's reagent, introducing the first stereoselective synthesis step.[31,32] Begley[33] and Jones[34] utilized truncated ferribactin derivatives for biomimetic oxidative cyclizations to the pyoverdin derivative.

Regarding their use as antimicrobials, siderophores and their iron-binding subunits seem to be highly attractive lead compounds for drug development.[10,35] However, combining a low molecular weight iron chelator with a macromolecular backbone is an effective strategy to limit the growth of pathogenic bacteria, because small iron binding molecules are likely to be ingested and digested by bacteria. Kizhakkedathu connected a hyperbranched polyglycerol with the hexadentate Fe(III) chelator *N*,*N*-bis(2-hydroxybenzyl)ethylenediamine-*N*,*N*-diacetic acid (HBED) units (subunit **6**, shown in Fig. 2).[36] These macromolecular Fe(III) chelators successfully slowed down the growth of *Staphylococcus aureus* and showed bactericidal activity when administered as adjuvants together with antibiotics.[36] An alternative approach was reported by Berkland who developed a biomimetic iron-sequestering polymer PAI-DHBA 7 *via* crosslinking of polyallylamine (PAI) with 2,3-dihydroxybenzoic acid (DHBA).[37] Pretreatment of culture media with this polymer effectively inhibited the growth of *Pseudomonas aeruginosa*.[37] Other catechol-based polymers with antibiotic activity against a

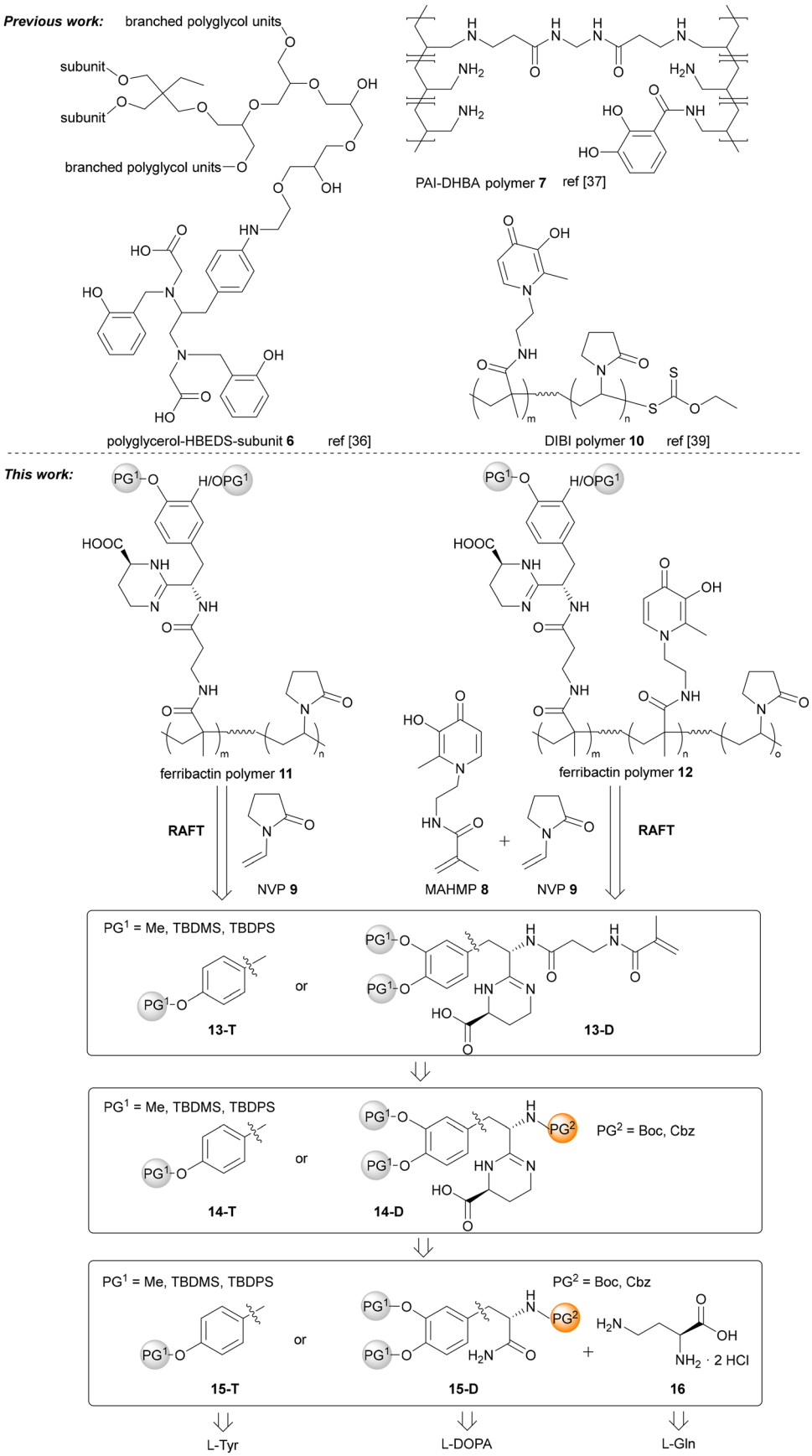

Fig. 2 Previous work on siderophore-polymer hybrids and the ferribactin-derived polymers described in this work.

variety of bacteria are known as well.[38] An attractive approach towards polymer-based drug delivery systems is the reversible addition–fragmentation chain transfer (RAFT) polymerization.[39–41] RAFT enabled, for example, the synthesis of amphiphilic copolymers with sequence-controlled alternating hydrophilic–hydrophobic pendant side chains.[42] Solvent-dependent self-assembly of these copolymers led to micelles, vesicles or reverse micelles, which were used for drug encapsulation.[42] Amino acid-based alternating copolymers displayed a pH-dependent reversal of amphiphilicity.[43,44] Previously, Ang *et al.* disclosed a deferiprone-functionalized acrylamide monomer **8** that was co-polymerized with *N*-vinylpyrrolidone **9** using RAFT polymerization to yield an iron-binding co-polymer, DIBI **10**, with enhanced antimicrobial activity.[45] The DIBI copolymer inhibited the growth of the antibiotic-resistant bacteria *Acinetobacter baumannii*, the methicillin-resistant *Staphylococcus aureus* as well as the yeasts *Candida albicans* and *Candida vini*.[46–48]

Our aim was to synthesize a library of polymerizable ferribactins with different protecting groups, to integrate them into polymers in order to obtain antibiotic polymers **11**, **12**, and to gauge the roles of the chromophores and pre-chromophores in the native compounds (Fig. 2). Although the synthesis of L-tyrosine-based ferribactin pre-chromophores **14-T** is known,[30,31] no synthetic route for the analogous L-DOPA-based derivatives **14-D** has been published yet. This should provide the basis for a biomimetic approach towards the pyoverdin chromophore **3-chr** *via* the ferribactin pre-chromophore **14-T** or **14-D** instead of truncated systems without stereogenic centers.[33,34] Since the synthesis route is complex, an incorporation of small amounts of the ferribactin-based monomers **13-T** and **13-D** with other easily available iron chelating monomers such as MAHMP **8** is favorable, to enhance the effects of already existing polymers. This was tested under the RAFT polymerization method that afforded the iron-chelating co-polymer DIBI.[45]

The ability to bind iron was evaluated by UV-vis measurements, a simpler and more sensitive method in comparison with NMR studies with Ga(III).[26] This should allow for better comparison between phenol- and catechol-derived ferribactins and different protecting groups, as well as a first indication of potential antimicrobial activity.

Finally, biological tests with synthesized ferribactins **13-T** and **13-D** and the obtained polymers **11** and **12** were performed with different bacteria to determine their antimicrobial activity. This data indicated the influence of structural motives in the ferribactins **13-T**, **13-D** and the incorporation into the polymers **11** and **12**, thus pointing to the first structure activity relationships (SAR).

2. Results and discussion

2.1. Retrosynthetic approach to the ferribactin pre-chromophore

In order to synthesize the ferribactin pre-chromophore derivatives **14-T** and **14-D**, the synthetic route *via* an iminoether, following a method by Jones[30] and Abdallah,[31] appeared to be the most promising (Fig. 2). The protection of the amino acid precursors was necessary for the synthesis of target polymers **11** and **12** in order to avoid undesired side reactions during the different synthetic steps. The set of *O*-methyl and *N*-Cbz protecting groups (PGs) was chosen to obtain chemically stable derivatives and to minimize accidental deprotection during acidic or other deprotecting reaction conditions throughout the planned synthetic route. But the deprotection of the methoxy ethers may not be viable for the target molecules **14-T** or **14-D** due to their stability. Therefore, another set, containing *O*-silyl and *N*-Boc protecting groups was chosen to synthesize derivatives that can be easily deprotected after synthesis of the target molecules **14-T** and **14-D**. Compounds **14-T**, **14-D** should be obtained *via* coupling of amides **15-T** and **15-D** with 2,4-diaminobutyric acid (DABA) **16** (prepared from L-glutamine **17**) and subsequent cyclization. Amides **15-T** and **15-D** should be synthesized from L-tyrosine **18a** and L-DOPA **18b**, respectively.

2.2. Synthesis of ferribactins derived from tyrosine and DOPA amides

First, the amide derivatives of L-tyrosine **18a** and L-DOPA **18b** had to be prepared. As shown in Scheme 1, the amino groups of L-tyrosine **18a** and L-DOPA **18b** were protected first by modification of known procedures.[49–51] Tyrosine **18a** was treated with Boc_2O and NaOH (method A) and gave Boc-tyrosine **19a-T** in quantitative yield, while the Boc protection of DOPA **18b** was performed with $NaHCO_3$ and Boc_2O and gave Boc-DOPA **19b-D** in quantitative yield (entries 1, 2). The Cbz protection of tyrosine **18a** was performed with CbzCl (method B) and yielded 53% of Cbz-tyrosine **19c-T**. The Cbz-DOPA **19d-D** was obtained in a similar reaction with CbzCl and K_2CO_3 in 48% (entries 3, 4). Then the vicinal hydroxy groups of the phenol moiety were protected with different protecting groups according to literature to avoid oxidation reactions towards quinoid systems.[50,52] Boc-DOPA **19b-D** was treated with TBDMSCl (method C) to give the TBDMS and Boc-protected **20b-D** in 43% yield (entry 5). The Cbz-protected tyrosine **19c-T** and DOPA **19d-D** were alkylated with an excess of MeI and the obtained methyl esters were saponified with 2 M NaOH to yield the *O*-methyl-*N*-Cbz-protected tyrosine **20c-T** in 80% and the *O*-methyl-*N*-Cbz-protected DOPA **20d-D** in 78%, respectively (method D, entries 6, 7).

The amidations of the protected derivatives **20b-D**, **20c-T** and **20d-D** were performed according to a modified procedure by Moreno-Cinos with isobutyl chloroformate and concentrated NH_3 solution, yielding the *O*-TBDMS-*N*-Boc-DOPA amide **15b-D** in 58%, the *O*-methyl-*N*-Cbz-tyrosine amide **15c-T** in 55% and the *O*-methyl-*N*-Cbz-DOPA amide **15d-D** in 49% respectively (method E, entries 9, 10, 11).[53] To obtain *O*-TBDPS-*N*-Boc-tyrosine amide **15a-T**, the *N*-Boc-tyrosine **19a-T** was first treated according to Moreno-Cinos, then with TBDPSCl, yielding 21% of **15a-T** over two steps (method F, then method G, entry 8, see SI, Chapter S3).[53]

2.3. Synthesis of coupling agent 2,4-diaminobutyric acid (DABA)

The second building block for the coupling of the tetrahydropyrimidine ring in **14-T** and **14-D** is 2,4-diaminobutyric acid (DABA) **16**. The synthesis of DABA **16** started with glutamine **17** (Scheme 2), which was treated with Boc_2O (analogue to tyrosine

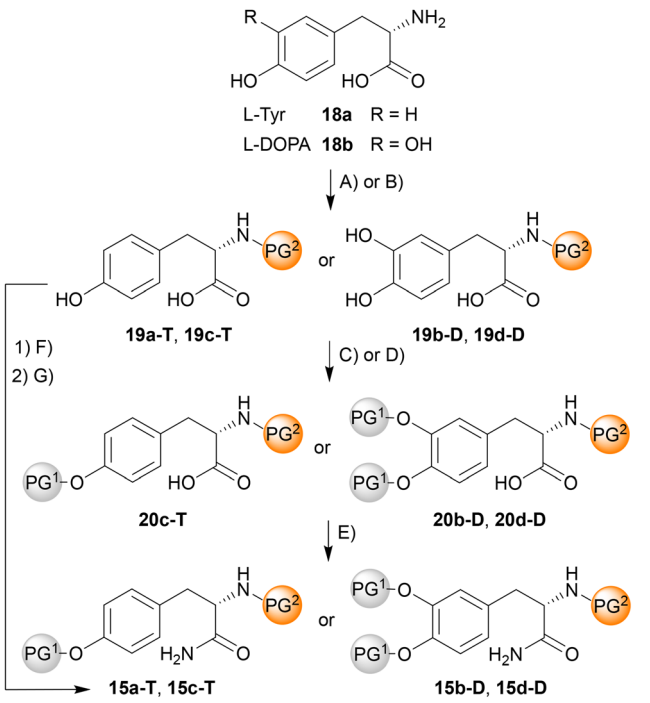

entry		PG^1	PG^2	method	yield [%]
1	**19a-T**	-	Boc	A	quant.
2	**19b-D**	-	Boc	A	quant.
3	**19c-T**	-	Cbz	B	53
4	**19d-D**	-	Cbz	B	48
5	**20b-D**	TBDMS	Boc	C	43
6	**20c-T**	Me	Cbz	D	80
7	**20d-D**	Me	Cbz	D	78
8	**15a-T**	TBDPS	Boc	F, G	21
9	**15b-D**	TBDMS	Boc	E	58
10	**15c-T**	Me	Cbz	E	55
11	**15d-D**	Me	Cbz	E	49

Scheme 1 Synthesis and results of tyrosine and DOPA amides. (A) Boc_2O, NaOH or $NaHCO_3$, H_2O, THF, rt, 22–25 h, quant.; (B) CbzCl, NaOH or K_2CO_3, H_2O, THF, rt, 23–26 h, 48–53%; (C) TBDMSCl, imidazole, MeCN, rt, 42 h, 43%; (D) MeI, K_2CO_3, DMF, rt, 18–26 h, then 2 m NaOH, rt, 6–19 h, 78–80%; (E) *N*-methylmorpholine, isobutyl chloroformate, concentrated NH_3, CH_2Cl_2, 0 °C to rt, 21–24 h, 49–58%, (F) *N*-methylmorpholine, isobutyl chloroformate, concentrated NH_3, CH_2Cl_2, 0 °C to rt, 18 h, then 1 M NaOH, THF, rt, 3 h, 54%; (G) **S3-T**, TBDPSCl, imidazole, CH_2Cl_2, rt, 25 h, 38%. For further details see Chapter S2, SI.

18a)[49] and Boc-glutamine **21** was isolated in 67% yield (method A). A Hofmann rearrangement with *N*-Boc-glutamine **21** was performed with Br_2 and NaOH, then the resulting intermediate was protected with Boc_2O, so *N,N*-Boc_2-DABA **22** could be obtained in 44% yield (method B).[54] Boc_2-DABA **22** was treated with an excess of concentrated HCl to yield DABA **16** as dihydrochloride in 84% (method C).[55]

2.4. Formation of ferribactin pre-chromophore monomers

After optimization (see SI, Chapter S3), pre-chromophore synthesis was performed according to Jones.[34] Therefore, the silyl-protected

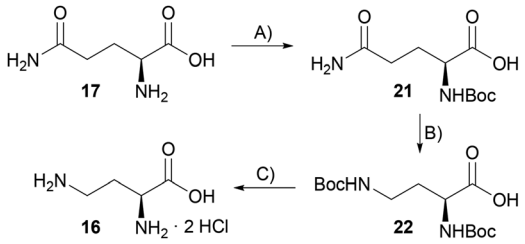

Scheme 2 Synthesis of DABA **16**. (A) Boc_2O, NaOH, H_2O, THF, rt, 22 h, 67%; (B) Br_2, NaOH, H_2O, 0 °C to 80 °C, 2 h, then Boc_2O, NaOH, H_2O, 1,4-dioxane, rt, 24 h, 44%; (C) concentrated HCl, rt, 2 h, 84%.

amines **15a-T**, **15b-D** and the methyl-protected amides **15c-T**, **15d-D** were stirred with MeOTf, then coupled with DABA **16** to obtain the corresponding ferribactin pre-chromophores (**14a-T**, **14b-D**, **14c-T**, **14d-D**) (Scheme 3). The silyl-protected derivatives yielded 94% for **14a-T** and 59% for **14b-D** (method A, entries 1, 2), while the methyl-protected derivatives yielded 73% for **14c-T** and 40% for **14d-D** (entry 3, 4).

For further functionalization to the ferribactin monomers **13a-T**, **13b-D**, **13c-T** and **13d-D** deprotection was necessary. For the silyl-protected, Boc-containing derivatives **14a-T** and **14b-D**, the acid-catalyzed reaction with trifluoroacetic acid (TFA) according to a method by Imramovský was successfully applied.[56] The derivatives **14a-T** and **14b-D** were deprotected with TFA and used without isolation in the subsequent coupling reaction.[57] Activation of *N*-Boc-protected β-alanine **S2** with EDC·HCl and HOBt, followed by addition of the deprotected derivatives of **14a-T** and **14b-D**, yielded the silyl-protected spacer derivatives **23a-T** in 83% and **23b-D** in 42% (method B, entries 5, 6). After optimization (see SI, Chapter S3), the method of Ghorai was used to deprotect the methylated Cbz-derivatives **14c-T** and **14d-D**.[58] Sequential treatment with 6 M HCl, then coupling with *N*-Boc-protected β-alanine **S2** yielded the methyl-protected compounds **23c-T** in 5% and **23d-D** in 35% respectively (method B, entries 7, 8).[58] To introduce the polymerizable side group, Boc deprotection with TFA was carried out on the silyl-protected (**23a-T**, **23b-D**) and methyl-protected (**23c-T**, **23d-D**) spacer derivatives. The subsequent coupling reaction (optimized as described in the SI, Chapter S3) was performed with methacrylic acid, EDC·HCl and HOBt. The silyl-protected monomers **13a-T** and **13b-D** were obtained in 80% and 49% yield. The methyl-protected monomers **13c-T** and **13d-D** were obtained in 68% and 47% yield (method C, entries 9, 10, 11, 12).

2.5. Investigation of iron binding properties of ferribactin pre-chromophore monomers

The silyl-protected (**13a-T**, **13b-D**) and methyl-protected (**13c-T**, **13d-D**) monomers were tested regarding their Fe(III)-binding properties by adding increasing amounts of $FeCl_3$ (4 mM solution in MeOH) to a solution of monomers in MeOH and monitoring the absorbance *via* UV-vis spectroscopy (Fig. 3). To study how the protecting groups alter the Fe(III)-binding properties, samples of the silyl-protected monomers **13a-T** and **13b-D** were deprotected with TBAF to yield deprotected **24a-T**

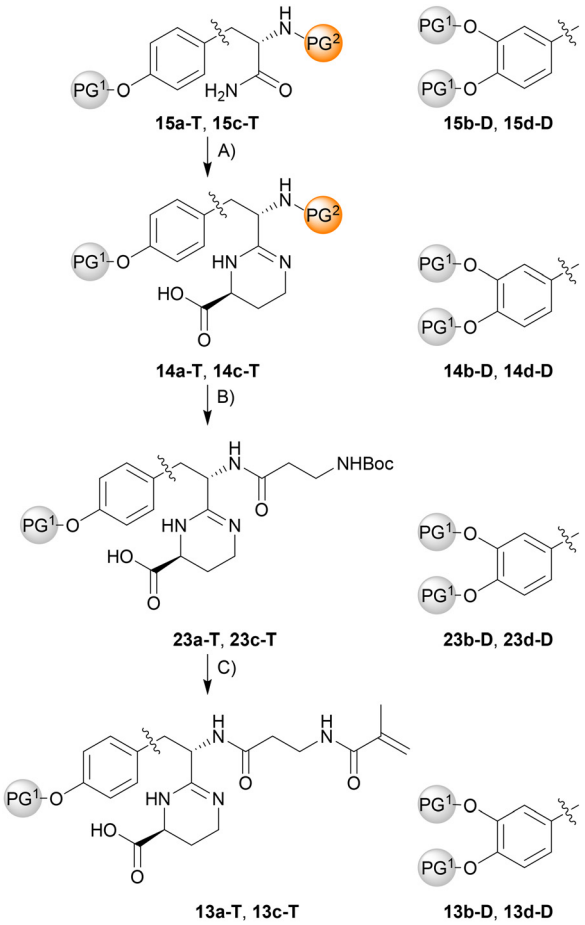

entry		PG^1	PG^2	method	yield [%]
1	**14a-T**	TBDPS	Boc	A	93
2	**14b-D**	TBDMS	Boc	A	59
3	**14c-T**	Me	Cbz	A	73
4	**14d-D**	Me	Cbz	A	40
5	**23a-T**	TBDPS	-	B	83
6	**23b-D**	TBDMS	-	B	42
7	**23c-T**	Me	-	B	5
8	**23d-D**	Me	-	B	35
9	**13a-T**	TBDPS	-	C	80
10	**13b-D**	TBDMS	-	C	49
11	**13c-T**	Me	-	C	68
12	**13d-D**	Me	-	C	47

Scheme 3 Coupling reaction to ferribactin pre-chromophores and modification to monomers. (A) MeOTf, CH_2Cl_2 or $CHCl_3$, reflux to rt, 22–27 h, then DABA **16**, iPr_2EtN, EtOH, rt to reflux, 20–23 h, 40–93%; (B) TFA, CH_2Cl_2, rt, 4 h or 6 M HCl, reflux, 6 h then Boc-β-alanine **S2** EDC·HCl, HOBt·H_2O, *N*-methylmorpholine, CH_2Cl_2 or DMF rt, 16–22 h, 5–83%; (C) TFA, CH_2Cl_2, rt, 2–4 h then methacrylic acid (MAA), EDC·HCl, HOBt·H_2O, N-methylmorpholine, CH_2Cl_2, rt, 16–23 h, 47–80%. For further details see Chapter S2, SI.

and **24b-D**. The TBAF was not removed before the measurements. In Fig. 3 the absorbance of all variants with an added amount of 80 nmol of Fe(III) in approx. 1 mL solvent is shown exemplarily (all spectra are shown in the SI, Fig. S2–S7). The enlarged section of the absorption spectrum at λ = 400–800 nm (Fig. 3b) shows that for all protected derivatives no additional band was detected as was expected for the Fe(III) binding according to the literature.[59–61] None of the protected monomers showed Fe(III) binding properties, even the sterically less demanding methyl ethers in **13d-D** were suppressing coordination. The phenol/catechol-unit of the molecule was proven to be the only binding site by detecting a shift in absorbance, although several peptide bonds and the tetrahydropyrimidine ring were present. The peptide bonds and the tetrahydropyrimidine ring remained unchanged and free during the complexation experiments. The deprotected **24b-D** (catechol-type) showed a wide band with a maximum absorbance around 570 nm, which indicates an Fe(III) binding at the catechol unit. This aligns perfectly with the ligand system containing two catechol units at neutral pH as reported by Bijlsma.[59] The deprotected **24a-T** (phenol-type) showed a narrow and much weaker band with a maximum absorbance at 460 nm, which would fit in the range of phenol-containing Fe(III) complexes.[60,61] Due to its small intensity, it is assumed that a very weak complexation occurred.

Since UV-vis measurements showed that the free catechol moiety is needed for Fe(III) binding, we surmised that the silyl-protected monomers (**13a-T**, **13b-D**) and the methyl-protected monomers (**13c-T**, **13d-D**) probably cannot induce a state of iron deficiency and show antimicrobial effects from iron depletion. Only the enzymatic catechol deprotection of the DOPA-derived derivatives **13b-D** (silyl-protected) or **13d-D** (methyl-protected) might lead to this effect. The Fe(III) binding of the tyrosine-based derivatives **13a-T** (silyl-protected), **13c-T** (methyl-protected) in their free phenolic form is probably too weak to show an effect. It can be concluded that the complexation behavior of ferribactin and polymer derivatives occurs through the catechol moiety, as there is an absence of metal complexation towards peptide bonds and the tetrahydropyrimidine.

2.6. Polymerization of ferribactin pre-chromophore monomers

Copolymerization of the silyl-protected monomers (**13a-T**, **13b-D**) and the methyl-protected monomers (**13c-T**, **13d-D**) with *N*-vinylpyrrolidinone (NVP) **9** and *N*-[2-(3-hydroxy-2-methyl-4-oxopyridin-1(4*H*)-yl)ethyl]methacrylamide (MAHMP) **8** was attempted. DIBI **10** was synthesized as a control reaction according to the original conditions by Ang[45] (Scheme 4), which yielded DIBI **10** in 83%, to show successful polymerization conditions and to obtain DIBI as non-(pre-)-chromophore containing co-polymer for control experiments.

The reaction conditions were adjusted for the silyl-protected (**13a-T**, **13b-D**) and methyl-protected (**13c-T**, **13d-D**) monomers as shown exemplarily for the polymerizations of methyl-protected **13c-T** in Scheme 4. The reactions were performed in μM scale in gas chromatography (GC) vials. The monomers, RAFT-agent **25**, NVP **9** and tetramethylethylenediamine (TMEDA) were dissolved in the solvent or solvent mixture (Table 1). Due to solubility issues we, unfortunately, could not use the reported RAFT conditions.[42–44] *Tert*-butyl hydroperoxide (TBHP) was added and stirred at 40 °C.

The methyl-protected monomers **13c-T** and **13d-D** were soluble in water. As shown in Table 1 (entry 1) and Scheme 4

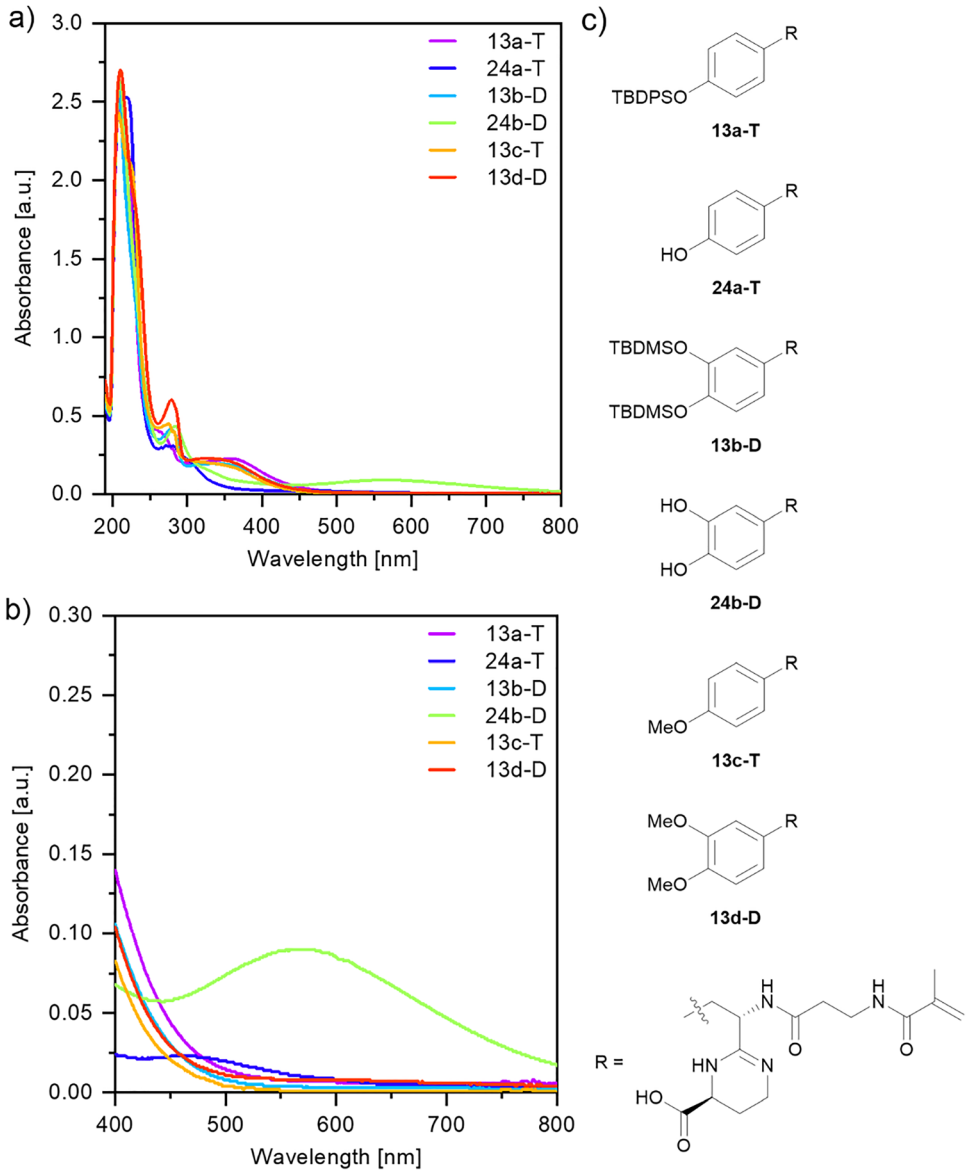

Fig. 3 (a) UV-vis spectra of 1 mL of stock solutions in MeOH with molar concentrations of **13a-T**: 64.9 μM, **13b-D**: 92.7 μM, **13c-T**: 122.5 μM, **13d-D**: 112.0 μM, **24a-T**: 64.9 μM (TBAF not removed), **24b-D**: 92.7 μM (TBAF not removed), with added 20 μL of 4 mM $FeCl_3$ solution (80 nmol $FeCl_3$); (b) Enlarged section of (a) at λ = 400–800 nm; (c) structures of **13a-T**, **13b-D**, **13c-T**, **13d-D** and **24a-T**, **24b-D**.

(middle), the methyl-protected monomer **13c-T** reacted with NVP **9** without further change to the reaction conditions of the DIBI **10** control and yielded polymer **11c-T** in 65%. Copolymerization of NVP **9** and MAHMP **8** (Scheme 4, bottom and Table 1, entry 2) was performed and yielded DIBI polymer **12c-T** in 71%, confirming reagent and reaction conditions. For the methyl-protected monomer **13d-D**, a similar reactivity was expected as compared to methyl-protected **13c-T**, but no reaction occurred under aqueous conditions (entry 3). Due to their hydrophobic protection groups, the silyl-protected monomers **13a-T** and **13b-D** could not be dissolved in H_2O, therefore addition of a co-solvent was necessary (entry 4). For silyl-protected **13a-T**, a mixture of H_2O and DMSO was tested and yielded a solid. The NMR spectrum of the solid showed an overlapping mixture of broadened singlets and sharp doublets of the tyrosine phenyl ring protons. The broadened singlets indicate polymerization and the remaining sharp doublets indicate that silyl-protected monomer **13a-T** is still present (see SI, page S158). Additionally, the matrix-assisted laser desorption (MALDI) mass spectra data shows no polymer distribution and only one relevant signal at 1156.98, since the mass of silyl-protected **13a-T** is 640.31 and the mass of NVP **9** is 111.07 (see SI, Chapter S13). We deduced from this data that the formation of short chains of oligomers had likely occurred (entry 5). The silyl-protected DOPA derivative **13b-D** did not show any reaction under the RAFT conditions. Silyl-protected **13b-D** gelled the (1 : 1) mixture of H_2O/DMSO as well as the (1 : 1) mixture of H_2O/DMF with the intended concentration of 26 mM while dissolving, before the start of the

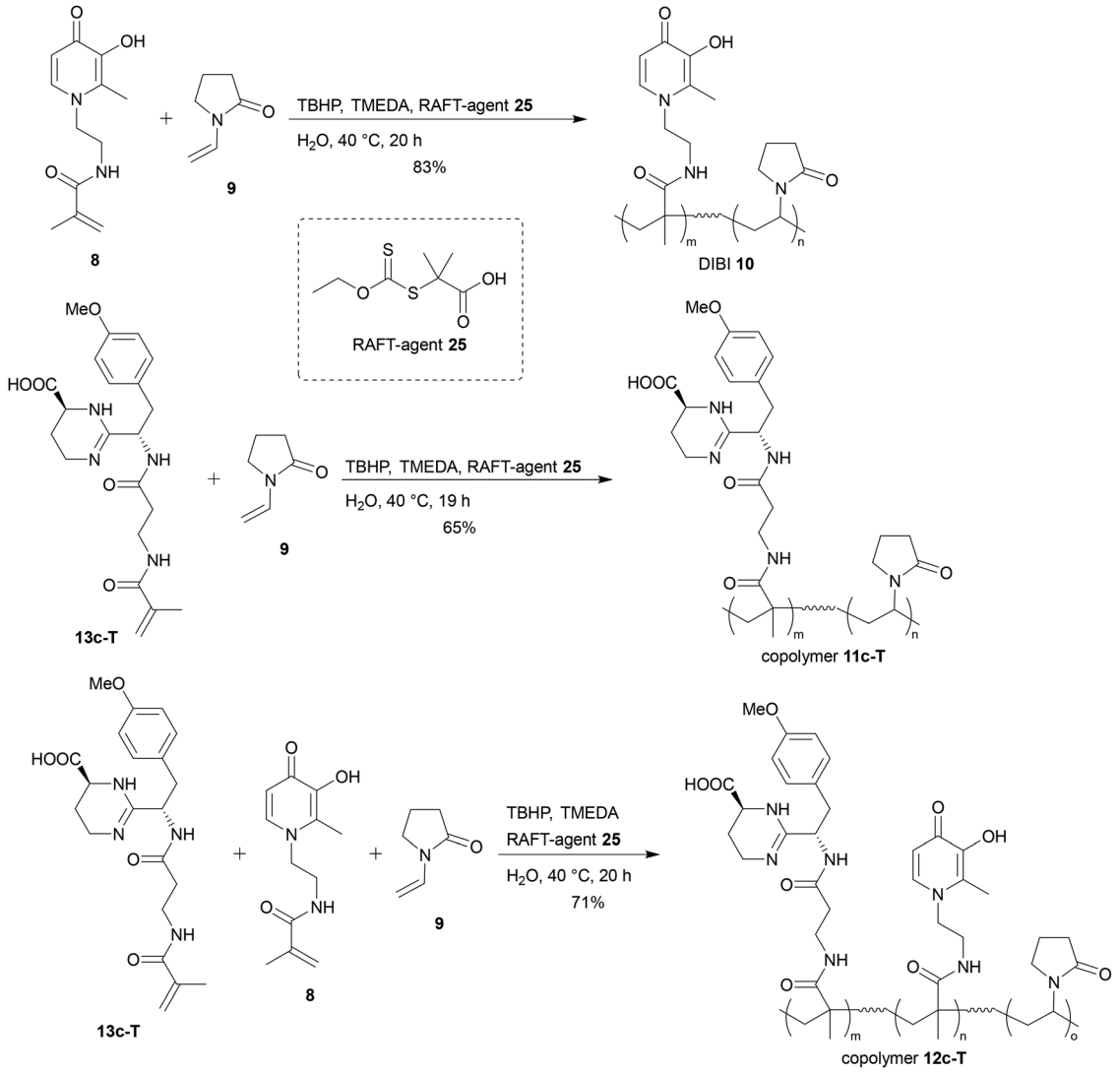

Scheme 4 Polymerization conditions towards DIBI **10** and methyl-protected **13c-T** with NVP (**9**), MAHMP (**8**), RAFT-agent (**25**), tetramethylethylenediamine (TMEDA) and *tert*-butyl hydroperoxide (TBHP).

Table 1 Reaction conditions for the polymerization attempts of silyl-protected (**13a-T**, **13b-D**) and methyl-protected (**13c-T**, **13d-D**) monomers with NVP **9** and MAHMP **8**

Entry	Monomer	Comonomer	Solvent (v : v)	Time [h]	Yield [%]	Observation
1	**13c-T**	NVP **9**	H_2O	19	65	copolymer **11c-T** formed
2	**13c-T**	NVP **9**, MAHMP **8**	H_2O	20	71	copolymer **12c-T** formed
3	**13d-D**	NVP **9**	H_2O	18	—	no reaction
4	**13a-T**	NVP **9**	H_2O	—	—	**13a-T** does not dissolve
5	**13a-T**	NVP **9**	H_2O/DMSO 1 : 1	18	—	oligomers formed
6	**13b-D**	NVP **9**	H_2O/DMSO 1 : 1	—	—	gelation of reaction mixture
7	**13b-D**	NVP **9**	H_2O/DMF 1 : 1	—	—	gelation of reaction mixture
8	**13b-D**	NVP **9**	Dioxane/H_2O 5 : 3	18	—	no reaction

reaction (entries 6, 7). The gelation of solvents by DOPA derivatives and short peptides containing DOPA is known.[62,63] Moreover Kar[64] observed the gelation of dioxane, THF, DMSO and DMF by TBDMS protected (catechol unit) DOPA, that was solely caused by the silyl units and showed liquefaction after cleavage of the TBDMS ether with fluoride. The silyl-protected monomer **13b-D** was soluble in a (5 : 3) mixture of 1,4-dioxane/H_2O, but the monomer showed no conversion under RAFT conditions (entry 8). Incorporation of silyl-protected monomers **13b-D** and **13a-T** as well as additional silyl deprotection was desirable. For silyl-protected **13b-D**, this would lead to a free catechol, that could bind iron (as shown for the deprotected

24b-D in chapter 2.5) or enhance the iron binding properties of existing polymers. Deprotected derivative **24a-T** could mimic ferribactin and deprotected derivative **24d-D** pyoverdin and their (pre-)chromophoric units, and, if recognized, interfere with the siderophore uptake of bacteria.

The co-polymerization with NVP **9** was performed to increase water solubility with the aim of increasing the iron binding and bioactivity of the silyl-protected monomers **13a-T** and **13b-D** and the methyl-protected monomers **13c-T** and **13d-D**. Poly-NVP polymers and co-polymers are known for their great water solubility and have been used as blood plasma extenders.[65] A polymer has additional advantages. It cannot be as easily taken up and digested by bacteria[36] and can improve the antibacterial activity with an effect of cooperation through several active units in the vicinity, as shown by Ang[45] in DIBI **10**. Another effect mentioned by Ang is the induction of steric hinderance by the polymer chain, later described as the polymer molecule wrapping around the Fe(III), that increases the antimicrobial effect.[45,47] All of these effects might combine in our targeted polymers. After polymerization, the silyl groups of the incorporated **13a-T** and **13b-D** could be deprotected to benefit from the iron binding capacity due to the free phenol or catechol moiety. The β-alanine as a short spacer was chosen to mirror the ethyl amide linker of MAHMP **8** and methacrylate as polymerizable group was used to get the same reactivity as MAHMP **8** by Ang, since the same polymerization method and conditions were chosen.[45] Increasing solubility by polymerization worked, because the obtained polymers **11c-T** and **12c-T** of the monomer **13c-T** were easily water soluble. Even the oligomers of silyl-protected **13a-T** with **9** showed an increased water solubility, compared with the silyl-protected monomer **13a-T** itself.

For the successfully synthesized polymers **10**, **11c-T** and **12c-T**, diffusion-ordered spectroscopy (DOSY) NMR spectra and MALDI mass spectra were measured (see SI, Chapter S7). For **10**, the MALDI distribution showed a maximum in the same order of magnitude as the molecular weight for **10** synthesized by Ang.[45] For **11c-T** and the mixed polymer **12c-T**, the maxima were lower. DOSY spectra are 2D spectra, showing the cross signals of the ^{1}H NMR and the diffusion coefficient (see SI, Table S2). No homopolymer formation for **10**, **11c-T** or **12c-T** was observed and the extracted diffusion coefficients lie roughly in between the reported ones for NVP **9** and PVP.[66]

2.7. Biological tests

The biological tests were performed in aqueous medium with small amounts of DMSO. Due to their solubility in H_2O and H_2O/DMSO mixtures, the silyl-protected monomers (**13a-T**, **13b-D**), the methyl-protected monomers (**13c-T**, **13d-D**) and the polymers (**11c-T**, **12c-T**) were chosen for biological testing. For comparison, the known DIBI polymer **10** was included in the assays.[45]

The cytotoxicity tests were performed with L929 mouse cells and the Alamar Blue assay was used to evaluate the viability of the cells.[67] As an example of the obtained results, the data for **13a-T** are shown in Fig. 4.

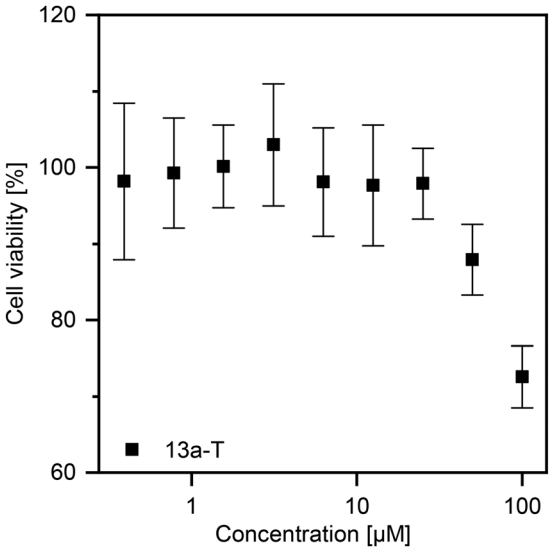

Fig. 4 Cell viability assay of the monomer **13a-T**.

The silyl-protected monomers **13a-T** and **13b-D** and the methyl-protected monomers **13c-T** and **13d-D** (see SI, Fig. S8) displayed a similar influence on cell viability regardless of the protecting groups. A variation of around 90% to 110% was obtained for concentrations from 0.4 μM to 25 μM, showing no cytotoxicity in this concentration range and lying within the expected experimental measurement error range. For concentrations higher than 50 μM, the cell viability decreased with increasing concentration (70% cell viability at 100 μM), indicating cytotoxic properties at higher concentrations. For polymers **11c-T**, **12c-T** and DIBI **10** the cell viability increased slightly with increasing concentrations (see SI, Fig. S9). The results indicated that the studied polymers **12c-T**, **11c-T** and DIBI **10** were not cytotoxic.

Antibacterial tests were performed with *Escherichia coli* wild type (WT), *Escherichia coli* ΔTolC, *Staphylococcus aureus*, *Klebsiella pneumoniae* and *Pseudomonas aeruginosa*. Four of which (*S. aureus, K. pneumoniae*, *P. aeruginosa, E. coli*) belong to the ESKAPE pathogens, which are representative for nosocomial multidrug resistant bacteria.[68] Examples for the results obtained are shown in Fig. 5 (For all results see SI, Fig. S10–S19).

For the *E. coli* WT no antibacterial activity of the silyl-protected monomers (**13a-T**, **13b-D**) and the methyl-protected monomers (**13c-T**, **13d-D**) was observed (Fig. S10). The polymers **10** and **12c-T** slightly inhibited growth of *E. coli* WT at the high concentrations of 50 μg mL^{-1} and 100 μg mL^{-1}, whereas the polymer **11c-T** showed no activity. This indicates that the activity is probably caused by the hydroxypyridone unit in the polymer **12c-T** (derived from monomer **8**), which agrees with the published results for DIBI **10**.[45] Presumably, at high concentrations both polymers created an iron poorer medium that led to decreased bacterial growth.

Next, tests were performed for *E. coli* ΔTolC. Since the ΔTolC mutant is defective in the TolC protein, which is in charge of the transport of molecules through the outer membrane, the results were expected to be more distinct.[69]

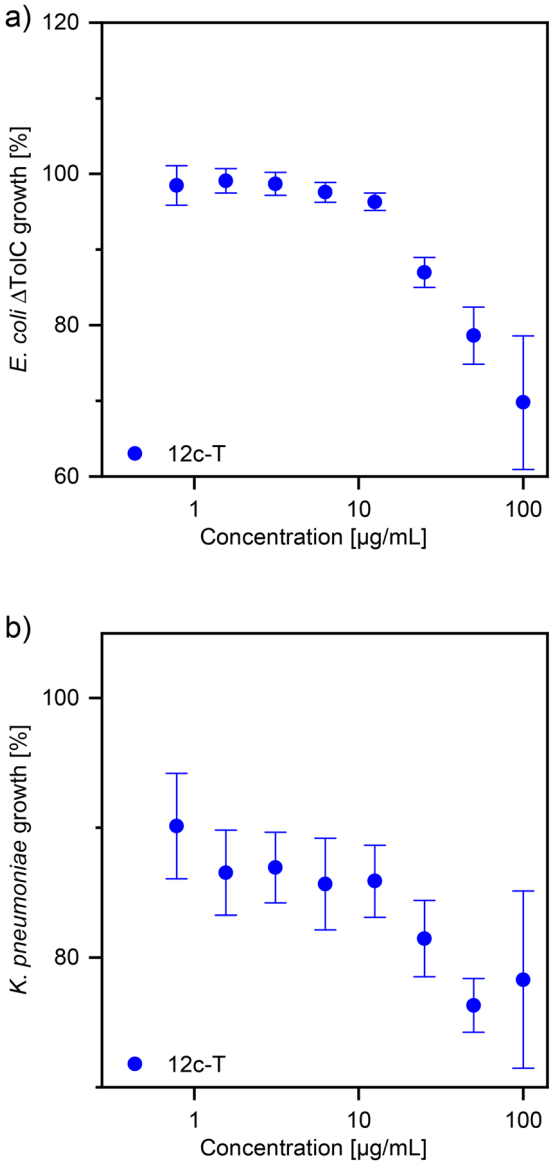

Fig. 5 Bacterial growth after incubation with **12c-T**. (a) *E. coli* ΔTolC, (b) *K. pneumoniae*.

The methyl-protected monomers **13c-T** and **13d-D** did not show any significant activity (Fig. S12). In contrast, the silyl-protected monomers **13a-T** and **13b-D** led to growth of about 80% at concentrations of 100 μM. Both monomers seem to be active against *E. coli* ΔTolC at high concentrations. As expected, the polymers showed a more distinct activity against the ΔTolC variant than against the wild type (Fig. S13). While **11c-T** had no activity, the polymers **10** and **12c-T** (Fig. 5a) reduced the growth of *E. coli* ΔTolC to 70–75%. The growth rate already decreased at concentrations of 10 μg mL^{-1}.

The tests with *S. aureus* showed no activity for the silyl-protected monomers (**13a-T**, **13b-D**) and the methyl-protected monomers (**13c-T**, **13d-D**) at low concentrations. Above 25 μg mL^{-1}, an increased growth of *S. aureus* occurred for all four monomers **13a-T**, **13b-D**, **13c-T** and **13d-D** (Fig. S14). This might be explained by metabolization of the monomers by the bacterium. However, this interpretation has to be approached with great care, because experimental edge effects might also be involved. The polymers **10** and **12c-T** had only little effect on the growth of *S. aureus* (Fig. S15), whereas **11c-T** showed a slight increase in growth at 100 μg mL^{-1}.

Tests with *K. pneumoniae* revealed increased bacterial growth with increasing concentration for the silyl-protected monomers (**13a-T**, **13b-D**) and for the methyl-protected monomer **13c-T**, while the methyl-protected monomer **13d-D** did not show any activity (Fig. S16). In comparison, the polymers **10**, **11c-T** and **12c-T** (Fig. 5b) slightly decreased growth (Fig. S17).

For *P. aeruginosa* no significant activity for the silyl-protected monomers (**13a-T**, **13b-D**) and the methyl-protected monomers (**13c-T**, **13d-D**) could be observed. The bacterial growth rate changed little irrespective of the concentrations (Fig. S18). Although the silyl-protected monomers (**13a-T**, **13b-D**) and the methyl-protected monomers (**13c-T**, **13d-D**) have a similar structure as the ferribactin pre-chromophore **4-chr**, no interference with bacterial biosynthesis seemed to occur. Presumably, the methoxy or silyloxy protecting groups are not cleaved by these bacteria. Neither polymer **12c-T** nor **11c-T** changed the growth of *P. aeruginosa* significantly, while DIBI **10** led to a slight decrease.

3. Conclusion

In conclusion, several protected ferribactin pre-chromophores were synthesized that, under the right conditions, can successfully be incorporated into polymers. Less polar monomers have lower solubility in water resulting in poor conversion during RAFT polymerization. UV-vis experiments showed that protected monomers cannot bind to iron. The unprotected catechol unit clearly shows iron binding behavior. We thus speculate that in naturally occurring iron-binding compounds, peptide polymer bonding and stabilization of the Fe(III) center is of little to no effect.

Biological tests showed no cytotoxicity at low concentrations but weak cytotoxicity at high concentrations, while the polymers showed no cytotoxic behavior. Non-cytotoxic properties are of interest for potential future antibacterial drug developments to selectively affect Fe(III) availability to pathogens and the human host.

Our results provided new ferribactin derivatives in monomeric form, which were embedded in a polymer. Future work is required to tackle the synthesis of polymers with deprotected ferribactin pre-chromophores and pyoverdin chromophore subunits, possibly through incorporation of protected precursors in the polymer in order to study their antibiotic potential and obtain detailed structure–activity relationships of these polymers.

Author contributions

A. P. G. synthesized the compounds and wrote the first draft of the manuscript. M. T. C. A. supervised the polymerization and

wrote the manuscript. S. H. helped with the pre-chromophore synthesis, B. N. G. and I. M. helped with the synthesis of precursors of the aza-Wittig route. D. C. M. C. performed the antibacterial tests, B. P. performed the cytotoxicity tests. U. B. supervised the biological testing and wrote the manuscript. M. B. supervised the polymerization and wrote the manuscript. A. Z. checked and managed the data. S. L. supervised the project and wrote the manuscript.

Conflicts of interest

There are no conflicts to declare.

Data availability

The data supporting the findings of this study are available within the article and its supplementary information (SI). Supplementary information is available. See DOI: **https://doi.org/10.1039/d5nj03251b**.

Additional raw data files are available from the corresponding author upon reasonable request.

Acknowledgements

The travel grant for A. Greulich by the Global Glimpse Fellowship Program of the University of Stuttgart as well as the Ministerium für Wissenschaft, Forschung und Kunst des Landes Baden-Württemberg, the European Regional Development Fund (EFRE, FEIH_778511), and the German Research Foundation DFG: Project-ID 358283783 – SFB 1333/2 2022 (for providing the infrastructure), HBFG shared instrumentation grants no. 513030456-INST 41/1175-1 FUGG for MALDI-MS, INST 41/897-1 FUGG for the 700 MHz NMR, INST 41/1136-1 FUGG for LC-Orbitrap-MS: Exactive Plus Orbitrap MS System and INST 41/1135-1 FUGG for GC-Orbitrap-MS: Exactive GC Orbitrap MS System are gratefully acknowledged. We acknowledge the support of Birgit Claasen and her department at the University of Stuttgart for all help surrounding NMR measurements and mass spectrometry. Thanks to Franziska Welsch and Ruben Pereira Rebelo from the University of Stuttgart for the MALDI measurements. The support of Friederike Adams with ideas for polymer analytics is acknowledged.

References

1 *World Health Organization, Global Antimicrobial Resistance and Use Surveillance System (GLASS)*, 2022, vol. 9.
2 I. N. Okeke, M. E. A. de Kraker, T. P. Van Boeckel, C. K. Kumar, H. Schmitt, A. C. Gales, S. Bertagnolio, M. Sharland and R. Laxminarayan, *Lancet*, 2024, **403**, 2426–2438.
3 S. K. Ahmed, S. Hussein, K. Qurbani, R. H. Ibrahim, A. Fareeq, K. A. Mahmood and M. G. Mohamed, *J. Med. Surg. Public Health*, 2024, **2**, 100081.
4 M. F. Chellat, L. Raguž and R. Riedl, *Angew. Chem., Int. Ed.*, 2016, **55**, 6600–6626.
5 G. Niro, S. C. Weck and C. Ducho, *Chem. – Eur. J.*, 2020, **26**, 16875–16887.
6 S. Kruth and M. Nett, *Antibiotics*, 2023, **12**, 1067.
7 M. Duplantier, E. Lohou and P. Sonnet, *Pharmaceuticals*, 2021, **14**, 1262.
8 J. Konstantinović, A. M. Kany, A. Alhayek, A. S. Abdelsamie, A. Sikandar, K. Voos, Y. Yao, A. Andreas, R. Shafiei, B. Loretz, E. Schönauer, R. Bals, H. Brandstetter, R. W. Hartmann, C. Ducho, C. M. Lehr, C. Beisswenger, R. Müller, K. Rox, J. Haupenthal and A. K. H. Hirsch, *ACS Cent. Sci.*, 2023, **9**, 2205–2215.
9 C. Jonkergouw, N. K. Beyeh, E. Osmekhina, K. Leskinen, S. M. Taimoory, D. Fedorov, E. Anaya-Plaza, M. A. Kostiainen, J. F. Trant, R. H. A. Ras, P. Saavalainen and M. B. Linder, *Nat. Commun.*, 2023, **14**, 2141.
10 U. Bilitewski, J. A. V. Blodgett, A. K. Duhme-Klair, S. Dallavalle, S. Laschat, A. Routledge and R. Schobert, *Angew. Chem., Int. Ed.*, 2017, **56**, 14360–14382.
11 M. Miethke and M. A. Marahiel, *Microbiol. Mol. Biol. Rev.*, 2007, **71**, 413–451.
12 R. Saha, N. Saha, R. S. Donofrio and L. L. Bestervelt, *J. Basic Microbiol.*, 2013, **53**, 303–317.
13 C. Rohrbacher, R. Zscherp, S. C. Weck, P. Klahn and C. Ducho, *Chem. – Eur. J.*, 2023, **29**, e202202408.
14 T. N. Pham, P. Loupias, A. Dassonville-Klimpt and P. Sonnet, *Med. Res. Rev.*, 2019, **39**, 2343–2396.
15 G. Briskot, K. Taraz and H. Budzikiewicz, *Z. Naturforsch., C: J. Biosci.*, 1986, **41**, 497–506.
16 H. Beiderbeck, D. Risse, H. Budzikiewicz and K. Taraz, *Z. Naturforsch., C: J. Biosci.*, 1999, **54**, 1–5.
17 C. Lenz, C. Amann, G. Briskot, K. Taraz and H. Budzikiewicz, *Z. Naturforsch., C: J. Biosci.*, 2000, **55**, 146–152.
18 A. M. Albrecht-Gary, S. Blanc, N. Rochel, A. Z. Ocaktan and M. A. Abdallah, *Inorg. Chem.*, 1994, **33**, 6391–6402.
19 C. Cezard, N. Farvacques and P. Sonnet, *Curr. Med. Chem.*, 2014, **22**, 165–186.
20 C. Cézard, P. Sonnet and B. Bouvier, *J. Biol. Inorg. Chem.*, 2019, **24**, 659–673.
21 P. Visca, F. Imperi and I. L. Lamont, *Trends Microbiol.*, 2007, **15**, 22–30.
22 R. Mashiach and M. M. Meijler, *Org. Lett.*, 2013, **15**, 1702–1705.
23 T. Kolasa and M. J. Miller, *J. Org. Chem.*, 1990, **55**, 4246–4255.
24 P. Seubert, M. Freund, R. Rudolf, Y. Lin, L. Altevogt, U. Bilitewski, A. Baro and S. Laschat, *Synlett*, 2020, 1177–1181.
25 T. Zhang, A. Bolhuis and I. M. Eggleston, *Eur. J. Org. Chem.*, 2024, e202400745.
26 K. Taraz, L. Seipold, C. Amann and H. Budzikiewicz, *Z. Naturforsch., C: J. Biosci.*, 2000, **55**, 836–839.
27 H. Budzikiewicz, M. Schäfer, D. U. Fernández, S. Matthijs and P. Cornelis, *Biometals*, 2007, **20**, 135–144.
28 U. Hohlneicher, M. Schäfer, R. Fuchs and H. Budzikiewicz, *Z. Naturforsch.*, 2001, **56c**, 308–310.
29 U. Hohlneicher, R. Hartmann, K. Taraz and H. Budzikiewicz, *Z. Naturforsch., C: J. Biosci.*, 1995, **50**, 337–344.

30 R. C. F. Jones and A. K. Crockett, *Tetrahedron Lett.*, 1993, **34**, 7459–7462.
31 A. Zamri, F. Sirockin and M. A. Abdallah, *Tetrahedron*, 1999, **55**, 5157–5170.
32 C. Hennard, Q. Chi Truong, J. F. Desnottes, J. M. Paris, N. J. Moreau and M. A. Abdallah, *J. Med. Chem.*, 2001, **44**, 2139–2151.
33 P. C. Dorrestein, K. Poole and T. P. Begley, *Org. Lett.*, 2003, **5**, 2215–2217.
34 R. C. F. Jones, S. C. Yau, J. N. Iley, J. E. Smith, J. Dickson, M. R. J. Elsegood, V. McKee and S. J. Coles, *Org. Lett.*, 2009, **11**, 1519–1522.
35 C. Kurth, H. Kage and M. Nett, *Org. Biomol. Chem.*, 2016, **14**, 8212–8227.
36 S. Abbina, A. Gill, S. Mathew, U. Abbasi and J. N. Kizhakkedathu, *ACS Appl. Mater. Interfaces*, 2020, **12**, 37834–37844.
37 N. El-Gendy, J. Qian, K. Eshelman, M. Rivera and C. Berkland, *Biomacromolecules*, 2015, **16**, 1480–1488.
38 S. Razaviamri, K. Wang, B. Liu and B. P. Lee, *Molecules*, 2021, **26**, 559.
39 D. J. Keddie, *Chem. Soc. Rev.*, 2014, **43**, 496–505.
40 M. D. Nothling, Q. Fu, A. Reyhani, S. Allison-Logan, K. Jung, J. Zhu, M. Kamigaito, C. Boyer and G. G. Qiao, *Adv. Sci.*, 2020, **7**, 2001656.
41 G. Moad, E. Rizzardo and S. H. Thang, *Chem. – Asian J.*, 2013, **8**, 1634–1644.
42 K. G. Goswami, S. Mete, S. S. Chaudhury, P. Sar, E. Ksendzov, C. Das Mukhopadhyay, S. V. Kostjuk and P. De, *ACS Appl. Polym. Mater.*, 2020, **2**, 2035–2045.
43 P. Sar, S. Ghosh, Y. D. Gordievskaya, K. G. Goswami, E. Y. Kramarenko and P. De, *Macromolecules*, 2019, **52**, 8346–8358.
44 P. Sar, S. G. Roy, P. De and S. Ghosh, *Macromol. Mater. Eng.*, 2020, **305**, 1900809.
45 M. T. C. Ang, R. Gumbau-Brisa, D. S. Allan, R. McDonald, M. J. Ferguson, B. E. Holbein and M. Bierenstiel, *Med. Chem. Commun.*, 2018, **9**, 1206–1212.
46 M. del C. Parquet, K. A. Savage, D. S. Allan, M. T. C. Ang, W. Chen, S. M. Logan and B. E. Holbein, *Antimicrob. Agents Chemother.*, 2019, **63**, 1–15.
47 M. del C. Parquet, K. A. Savage, D. S. Allan, R. J. Davidson and B. E. Holbein, *Front. Microbiol.*, 2018, **9**, 1–11.
48 B. E. Holbein and R. Mira De Orduña, *FEMS Microbiol. Lett.*, 2010, **307**, 19–24.
49 N. A. Bindman, S. C. Bobeica, W. R. Liu and W. A. Van Der Donk, *J. Am. Chem. Soc.*, 2015, **137**, 6975–6978.
50 M. J. Sever and J. J. Wilker, *Tetrahedron*, 2001, **57**, 6139–6146.
51 M. Li, B. Luo, Q. Liu, Y. Hu, A. Ganesan, P. Huang and S. Wen, *Org. Lett.*, 2014, **16**, 10–13.
52 J. P. T. A. Guerra, A. Lindner, C. R. Nicoleti, V. G. Marini, M. Silva and V. G. Machado, *Tetrahedron Lett.*, 2015, **56**, 4733–4736.
53 C. Moreno-Cinos, E. Sassetti, I. G. Salado, G. Witt, S. Benramdane, L. Reinhardt, C. D. Cruz, J. Joossens, P. Van Der Veken, H. Brötz-Oesterhelt, P. Tammela, M. Winterhalter, P. Gribbon, B. Windshügel and K. Augustyns, *J. Med. Chem.*, 2019, **62**, 774–797.
54 B. C. Askew, R. A. Bednar, B. Bednar, D. A. Claremon, J. J. Cook, C. J. McIntyre, C. A. Hunt, R. J. Gould, R. J. Lynch, J. J. Lynch, S. L. Gaul, M. T. Stranieri, G. R. Sitko, M. A. Holahan, J. D. Glass, T. Hamill, L. M. Gorham, T. Prueksaritanont, J. J. Baldwin and G. D. Hartman, *J. Med. Chem.*, 1997, **40**, 1779–1788.
55 M. Đud, Z. Glasovac and D. Margetić, *Tetrahedron*, 2019, **75**, 109–115.
56 R. Jorda, J. Dušek, E. Řezníčková, K. Pauk, P. P. Magar, A. Imramovský and V. Kryštof, *Eur. J. Med. Chem.*, 2017, **135**, 142–158.
57 W. J. Wu, Y. Wu and B. Liu, *Tetrahedron*, 2017, **73**, 1265–1274.
58 B. G. Das and P. Ghorai, *Chem. Commun.*, 2012, **48**, 8276–8278.
59 J. Bijlsma, W. J. C. de Bruijn, J. A. Hageman, P. Goos, K. P. Velikov and J. P. Vincken, *Sci. Rep.*, 2020, **10**, 1–11.
60 M. Emami, R. Bikas, N. Noshiranzadeh, J. Sanchiz, K. Ślepokura and T. Lis, *J. Mol. Struct.*, 2019, **1180**, 392–398.
61 B. K. Kanungo, M. Baral, S. K. Sahoo and S. E. Muthu, *Spectrochim. Acta, Part A*, 2009, **74**, 544–552.
62 D. Giuri, P. Ravarino and C. Tomasini, *Org. Biomol. Chem.*, 2021, **19**, 4622–4636.
63 D. Giuri, N. Zanna and C. Tomasini, *Gels*, 2019, **5**, 27.
64 S. K. Mandal, P. Seth and T. Kar, *New J. Chem.*, 2024, **48**, 5429–5438.
65 M. Teodorescu and M. Bercea, *Polym. Plast. Technol. Eng.*, 2015, **54**, 923–943.
66 N. T. M. Hai, J. Furrer, F. Stricker, T. M. T. Huynh, I. Gjuroski, N. Luedi, T. Brunner, F. Weiss, A. Fluegel, M. Arnold, I. Chang, D. Mayer and P. Broekmann, *J. Electrochem. Soc.*, 2013, **160**, D3116–D3125.
67 J. O'Brien, I. Wilson, T. Orton and F. Pognan, *Eur. J. Biochem.*, 2000, **267**, 5421–5426.
68 W. R. Miller and C. A. Arias, *Nat. Rev. Microbiol.*, 2024, **22**, 598–616.
69 G. Dhamdhere and H. I. Zgurskaya, *Mol. Microbiol.*, 2010, **77**, 743–754.

